Research Article | Vol. 1, No. 4 | 15 Dec 2018 | OSA CONTINUUM 1341
OSA CONTINUUM

Generation of a terahertz collimated top-hat beam by using two thin diffractive phase plates

XI YE, FEIDI XIANG, CHENGWU YOU, KEJIA WANG,* ZHENGANG YANG, JINSONG LIU, AND SHENGLIE WANG

Wuhan National Laboratory for Optoelectronics, School of Optical and Electronic Information, Huazhong University of Science and Technology, Wuhan 430074, Hubei, China
**wkjtode@sina.com*

Abstract: We propose an efficient approach for shaping a terahertz (THz) Gaussian beam to a collimated top-hat beam by using two thin diffractive phase plates. The phase plates are designed based on the phase retrieve algorithm and fabricated by well-developed 3D-printing technology. The designed THz top-hat beam is experimentally realized at 0.3-THz. Both the calculated root mean square (RMS) uniformity and fraction of the total beam power of the output top-hat beam are over 80%, respectively. Additionally, the comparison between our approach and the traditional system containing of two refractive aspheric lenses is performed, showing that our beam shaping system has higher energy utilization.

1. Introduction

In the past decade, various THz real-time imaging systems have advanced significantly [1–3]. These THz imagers have been already used in some area, e.g. security screening [4], non-destructive test of composite materials [5] and the investigation of cultural relics [6]. It is worthy noted that most of the mentioned THz imager are active. Thus the illumination module in system is a key issue for the acquisition of an image with high quality. As we known, THz wave emitted from a source usually has a Gaussian transverse profile that results a non-uniform illumination in the active imager.

In optics, a top-hat beam has a uniform intensity within a certain area, which can be formed by the refractive optical elements or the other phase devices [7,8]. Due to its homogeneous distribution of intensity, the top-hat beam is a desirable light source for an active imaging system [9]. In 2010, Kleindienst et al firstly proposed a method to obtain THz top-hat beam for a compact THz imager [9]. Specifically, they designed a single-element refractive beam shaper, converting the incidence Gaussian beam to a top-hat beam with Super-Gaussian intensity distribution. Their Gaussian-to-top-hat beam shaper was fabricated by milling the polypropylene substrate. Although the experimental results verified its feasibility, there were a few of problems about their approach that should be addressed.

Firstly, the intensity profile of output top-hat beam will deform quickly after the single-element beam shaper because of its non-uniform phase distribution [10], which limits its application in imaging with large depth of field. Besides, their Gaussian-to-top-hat beam shaper is a refractive element. As we known, the refractive element has higher absorption than the diffractive element due to its very thick size. Although the refractive element can be changed to a diffractive one based on the equivalency between phase shift and optical path [11,12], diffractive element cannot be easily or quickly fabricated by traditional processing technology for THz waves, such as milling or casting, because it has very complicated surface structure [9].

In 1991, Roux indicated that it was able to realize the intensity redistribution of any rotationally symmetric beam by using two diffractive optics elements. The first one diffracts

#347807 https://doi.org/10.1364/OSAC.1.001341
Journal © 2018 Received 9 Oct 2018; revised 12 Nov 2018; accepted 13 Nov 2018; published 11 Dec 2018

OSA CONTINUUM

incident light beam to generate desired output distribution. The second element is used to eliminate the non-uniform phase distribution in the output plane, keeping the top-hat distribution unchanged at a distance [10]. Using phase-only liquid crystal spatial light modulators (LC-SLMs) [8] or computer-generated holograms (CGHs) [13], one can easily obtain optical top-hat beam. Inspired by this approach, here we propose a beam shaping system containing of two diffractive thin phase plates (Fig. 1) to generate THz top-hat beam. In details, we firstly took a fast and efficient input-output algorithm to design the phase plates. Then we chose well-developed 3D-printing technology to fabricate these two phase plates with complex surface structure since there is no well-developed CGHs or SLMs for THz waves [12,14]. Based on the printed phase plates, the desired THz top-hat beam was experimentally realized at 0.3-THz. Finally, we compared the THz top-hat beam generated by our approach with that generated by two refractive aspheric lenses.

2. Design and fabrication of phase plates

The first step for the generation of top-hat beam is to select the output intensity profile. Shealy et al. concluded that flattened profiles can conform to four special functions: super-Gaussian, flattened Gaussian, Fermi-Dirac and super-Lorentzian. Note that these four top-hat beams are very similar to each other, i.e. they may not be distinguished in experiments [15]. In this paper, we choose a modified super-Lorentzian function, i.e. a Flattened-Lorentzian function, as our desired beam profile because the ray mapping functions can be solved analytically based on this function [16]. The normalized intensity profile of a Flattened-Lorentzian top-hat beam in radial coordinate is expressed as:

$$I_{p_2'}(r) = \frac{1}{\pi R_{FL}^2 \left[1+\left(r/R_{FL}\right)^q\right]^{1+2/q}}. \tag{1}$$

where r is the radius of polar coordinate system and R_{FL} denotes the half width at half maximum (HWHM) of profile. The q is the shaping parameter, with increasing which the edge of top-hat beam will be steeper.

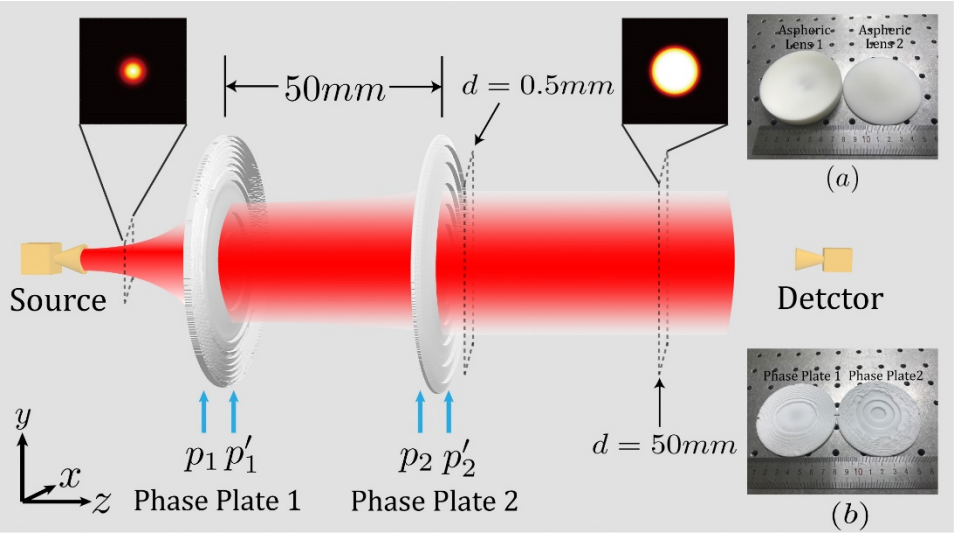

Fig. 1. Configuration of THz top-hat beam shaping system with two optical elements, (a). 3D-printed refractive aspheric lenses, (b). 3D-printed diffractive phase plates.

Our beam shaping system is illustrated in Fig. 1, converting a non-collimated THz Gaussian beam emitted from a source to the collimated THz top-hat beam directly. The

OSA CONTINUUM

distance of two elements is $50mm$ .The key process in the design is to obtain the phase distribution at the entrance surface p_1 (p_2) and exit surface p_1' (p_2') of the first (second) phase plate, respectively. Based on the thin lens approximation, we assume that the phase plates only change the phase distribution of beam while the intensity distribution will remain unchanged. Mathematically, the surface p_1 and p_1' share same spatial coordinate during the calculation, so do the surface p_2 and p_2' .

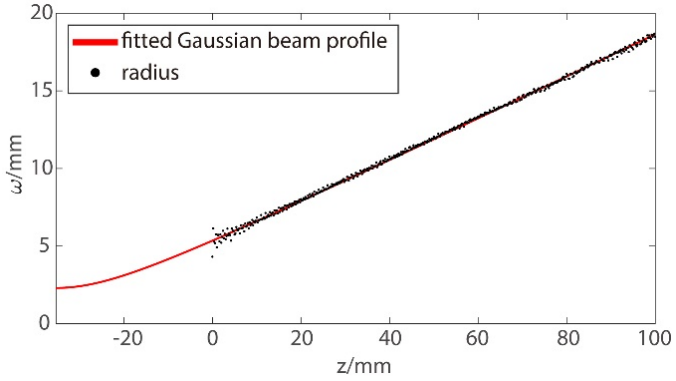

Fig. 2. The measured and fitting beam radius of THz Gaussian beam.

The source used in the following experiments is a Gunn-diode (Spacek Lab Inc.) driving multiplier-chain (Virginia Diode Inc.), delivering continuous wave radiation at 0.3-THz with output power of 0.3mW. In order to model the emitted THz Gaussian beam, we firstly measure the vertical angular intensity distribution and horizontal angular intensity distribution along the z -axis. Based on the measured results, the 0.3-THz beam radius (at which the beam intensity has fallen to $1/e^2$ of its peak) can be calculated and plotted by the black dot line in Fig. 2. According to the classical theory of Gaussian beam propagation, we can fit the beam radius, see the red line in Fig. 2. The modeled THz Gaussian beam for our design has a radius of beam waist $\omega_0 = 2.3mm$ located at $z_0 = -35.29mm$.

Based on the fitting results, we choose the x-y plane located at $z = 40mm$ as the entrance surface p_1 of the first phase plate. Figure 3 (a) is the measured intensity of emitted THz beam at this x-y plane, which will be used as the intensity distribution $I_{p_1}(r)$ in all following calculations. Note that measured horizontal angular intensity of THz beam, i.e. the black dot line shown in Fig. 3(b), is not a perfect Gaussian distribution. We believe that this distortion of emitted beam is caused by the slight mismatch of diagonal horn antenna on the emitter.

For a Gaussian beam, its phase fronts at the waist possess a constant profile. Since the radius of beam waist ω_0 and its location z_0 are already known, we can calculate the phase distribution φ_{p_1} at the surface p_1 based on angular spectrum transform (AST) [11], see Fig. 3(c).

Considering the radius of THz Gaussian beam at $z = 40mm$ is $R_0 = 11mm$, we set the shaping parameters of desired flat-top beam to be $q = 15$ and $R_{FL} = 20mm$ in Eq. (1). Thus the normalized ideal flat-top beam intensity $I_{p_2'}(r)$ can be obtained based on Eq. (1), as shown in Fig. 3(d) and (e). On the other hand, the phase distribution at p_2' is uniform (i.e. being a constant shown in Fig. 3 (f)) since the designed output beam is a collimated top-hat beam with plane wave fronts.

OSA CONTINUUM

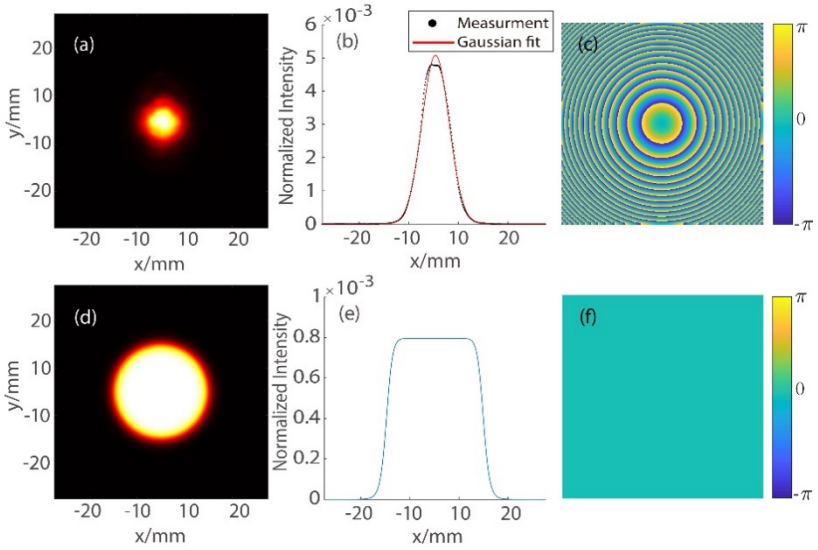

Fig. 3. (a). Measured normalized intensity distribution of THz source at $z = 40mm$; (b). Measured and fitting normalized Gaussian horizontal angular intensity of THz source at $z = 40mm$; (c). Calculated phase distribution at the surface p_1 ; (d). Calculated normalized intensity distribution of designed flat-top beam; (e). Calculated normalized horizontal angular intensity of designed flat-top beam; (f). Calculated phase distribution at the surface p_2' .

Based on above-mentioned assumption, we can get $I_{p_1}(r)=I_{p_1'}(r)$ and $I_{p_2}(r)=I_{p_2'}(r)$. Besides, the phase distribution at the surface p_1 and p_2' are fully known. So the remaining problems are focused on retrieving the phase distribution at p_1' and p_2 . Next we will use the phase retrieval algorithms to solve them.

In present day, there are many phase retrieval algorithms, such as prototype Gerchberg-Saxton algorithm [17], input-output algorithm [18] and Yang-Gu algorithm [19]. Here we will use the input-output algorithm because it can improve the convergence speed of prototype Gerchberg-Saxton algorithm [18]. In addition, the Fourier transform used in original input-output algorithm is changed to the AST for our design [20].

Since the input-output method is an iterative algorithm, we assume the complex amplitude of the kth iteration to be $\hat{U}_{p_1'}^k = \hat{A}_{p_1'}^k \exp(i\hat{\varphi}_{p_1'}^k)$ ($\hat{U}_{p_2}^k = \hat{A}_{p_2}^k \exp(i\hat{\varphi}_{p_2}^k)$) at p_1' (p_2), where $\hat{A}_{p_1'}^k$ ($\hat{A}_{p_2}^k$) and $\hat{\varphi}_{p_1'}^k$ ($\hat{\varphi}_{p_2}^k$) are the kth estimated amplitude and phase, respectively. For the first iteration ($k=0$), we assume that $\hat{A}_{p_1'}^0 = \sqrt{I_{p_1'}(r)}$, and $\hat{\varphi}_{p_1'}^0$ is chosen to be the phase delay of first aspheric lens designed by Kreuzer's method [7]. Applying AST [11], we can calculate the complex amplitude of the first iteration $\hat{U}_{p_2}^0 = \hat{A}_{p_2}^0 \exp(i\hat{\varphi}_{p_2}^0)$ at p_2 . Next is the key step: i.e. changing $\hat{A}_{p_2}^0$ to be $A_{p_2}^0 = \sqrt{I_{p_2}(r)}$ in which $I_{p_2}(r)$ has been obtained before. Substituting the modified $U_{p_2}^0 = A_{p_2}^0 \exp(i\hat{\varphi}_{p_2}^0)$ into AST, we calculate $\hat{U}_{p_1'}^1 = \hat{A}_{p_1'}^1 \exp(i\hat{\varphi}_{p_1'}^1)$. Then we modify $\hat{U}_{p_1'}^1$ to be $U_{p_1'}^1$ for the initial complex amplitude of next iteration ($k=1$) based on this equation [21]:

OSA CONTINUUM

$$U_{p_1'}^{k} = \hat{U}_{p_1'}^{k} + \left(\frac{\sqrt{I_{p_1'}(r)}}{\hat{A}_{p_1'}^{k}} - 1 \right) \hat{U}_{p_1'}^{k} + \left(\frac{\sqrt{I_{p_1'}(r)}}{\hat{A}_{p_1'}^{k}} \hat{U}_{p_1'}^{k} - \frac{\sqrt{I_{p_1'}(r)}}{\hat{A}_{p_1'}^{k\text{-}1}} \hat{U}_{p_1'}^{k\text{-}1} \right) \tag{2}$$

Repeating the above steps, we can retrieve the phase distribution at p_1' and p_2. The calculation will be stopped until the mean squared error between $\hat{A}_{p_1'}^{k}$ and $\hat{A}_{p_1'}^{0} = \sqrt{I_{p_1'}(r)}$ is small enough. Figure 4 illustrate the results with 3000 iterations, in which the calculating error is $5.2873e^{-4}$.

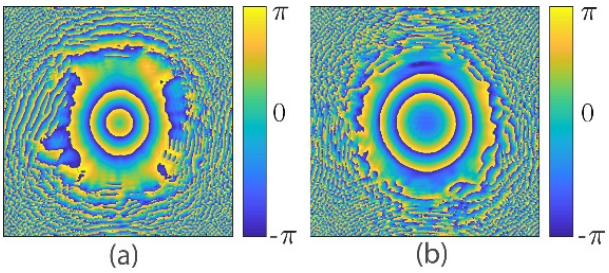

Fig. 4. The calculated phase distribution at the surface (a). p_1 and (b). p_2', respectively.

Now we have already obtained the phase distribution at the surface p_1, p_1', p_2 and p_2', based on which the phase plates can be designed by SolidWorks. Using a commercial 3D-printer (Objet30 Pro, Stratasys Ltd.) with a resolution of $42\mu m$ in x and y direction and $28\mu m$ in z direction, we can fabricate them no more than three hours, see Fig. 1 (a). The refractive index and absorption coefficient of the printing polymer material are 1.655 and $1.5cm^{-1}$, respectively [14]. These two phase plates have a diameter of $80mm$ and maximum thickness of $2.369mm$. Due to the phase dislocations produced by the phase retrieve algorithm [22], there are some irregular fluctuations on the phase plates. Note that the input Gaussian beam had a diameter of $20mm$ and output flat top beam had a diameter of $40mm$, which are both much smaller than the $80mm$ diameter of printed phase plates. Thus such phase dislocations have a little of effect on the experimental results.

The THz detector used in our characterization system of top-hat beam is a Schottky-diode (Virginia Diodes Inc.) in combination with an identical diagonal horn antenna, which is mounted on a motorized three-axis translation stage. The motor step is set to obtain a spatial resolution of $0.2mm$.

3. Experimental results and discussions

Figure 5 (a) and (d) illustrate the measured intensities of THz beam in x-y plane at distance of $d = 0.5mm$ and $50mm$, respectively. These experimental results show that the output beam has a quasi-homogenous intensity distribution with some small ripples. Besides, the output beam is collimated well between $d = 0.5mm$ and $d = 50mm$ because the beam size of Fig. 5 (a) and Fig. 5 (d) are close to each other. The Fig. 5 (b), (c), (e) and (f) illustrate that the measured results are matched with simulation. The diameter of generated THz top-hat beam is almost $40mm$.

In order to evaluate the performance of our shaping system, we quantitatively analyzed the results by using the method in [23]. Thus some quantities will be introduced. The first one is the average of intensity $\overline{I}$ within the aperture, written as:

$$\overline{I} = \frac{2}{R_{SL}^2} \int_0^{R_{SL}} I(r) r dr. \tag{3}$$

OSA CONTINUUM

The second one is the variance of intensity σ_I, written as:

$$\sigma_I = \frac{2}{R_{SL}^2}\int_0^{R_{SL}} [I(r)-\bar{I}]^2 rdr. \quad (4)$$

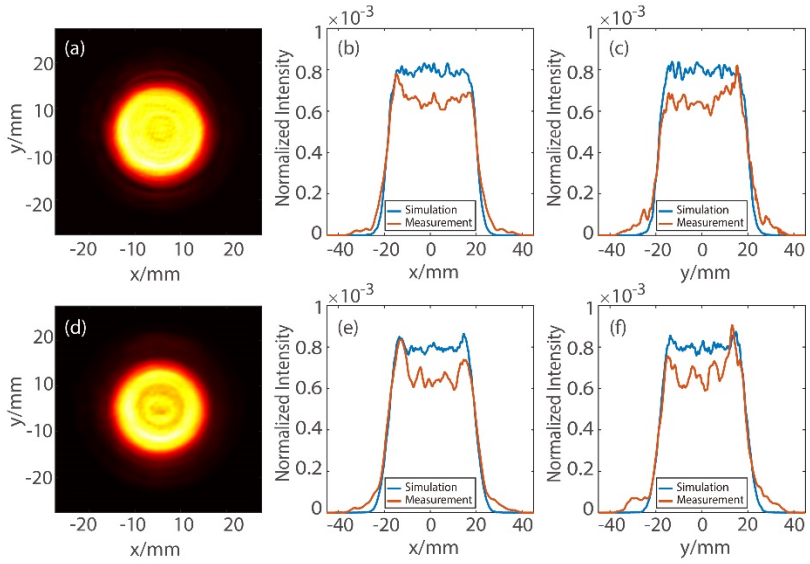

Fig. 5. (a). Experimental normalized intensity distribution in x-y plane at $d = 0.5mm$; (b). Experimental and simulation horizontal angular intensity at $d = 0.5mm$; (c). Experimental and simulation vertical angular intensity at $d = 0.5mm$; (d). Experimental normalized intensity distribution in x-y plane at $d = 50mm$; (e). Experimental and simulation horizontal angular intensity at $d = 50mm$; (f). Experimental and simulation vertical angular intensity at $d = 50mm$.

A relative RMS uniformity is defined as $U_{RMS} = 1-\sigma/\bar{I}$. And a fraction of the total beam power (FTBP) is written as $\eta = 2\pi\int_0^{R_{SL}} I(r)rdr$, where $I(r)$ is the normalized intensity distribution. Both U_{RMS} and η range from 0 and 1, with larger values being more desirable [22]. At $d = 0.5mm$, the calculated results are U_{RMS}=0.8424 (U_{RMS}=0.8231) and $\eta = 0.8021$ ($\eta = 0.9066$) for experiments (simulation), respectively. While at $d = 50mm$, the measured (simulated) results are U_{RMS}=0.8002 (U_{RMS}=0.7804) and $\eta = 0.7921$ ($\eta = 0.8953$), respectively. Thus the uniformity and FTBP of top-hat beam within the region $0 < r < R_{SL}$ will decrease as it propagates from near field to far field. Considering the experimental error, e.g. the fabrication error of 3D printing and displacement error of phase plates, our experimental results are consistent with design.

Besides, we also design a 3D-printed refractive aspheric lenses (Fig. 1(b)) system based on Kreuzer's method [7] for comparison. All experimental parameters are set to be same as the former diffractive phase plates system. The maximum thickness of two aspheric lenses is $13.87mm$. Note that this system has an additional plano-convex lens with a focal length of $50mm$ because the Kreuzer's method requires a collimated incident Gaussian beam. The measured and simulated results are illustrated in Fig. 6. At $d = 0.5mm$ ($d = 50mm$), the calculated U_{RMS}=0.7826 (U_{RMS}=0.8307) and $\eta = 0.6482$ ($\eta = 0.6033$), respectively. It is

OSA CONTINUUM

clearly that the output beam intensity of the aspheric lens system is twenty times smaller than that of the diffractive phase plates system due to the much higher absorption of thick aspheric lens.

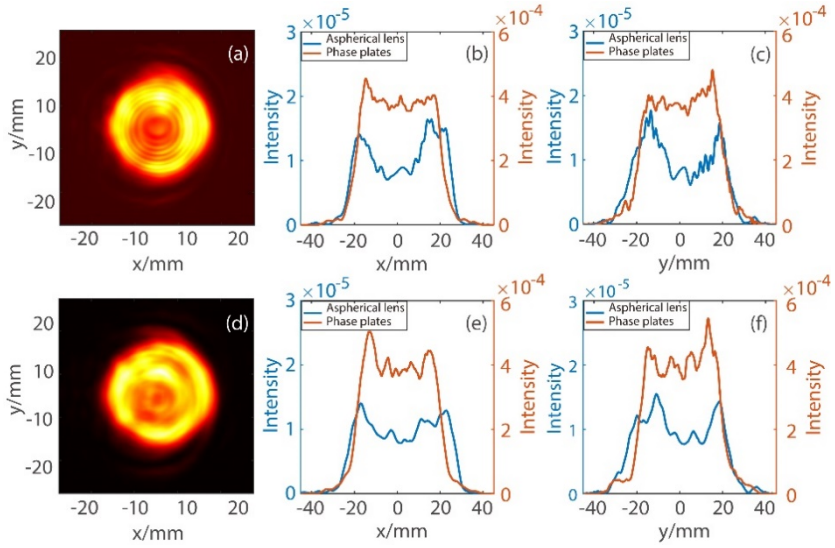

Fig. 6. Aspheric lens system experimental result; (a). Intensity distribution at $d = 0.5mm$; (b). Horizontal angular intensity at $d = 0.5mm$; (c). Vertical angular intensity at $d = 0.5mm$; (d). Intensity distribution at $d = 50mm$; (e). Horizontal angular intensity at $d = 50mm$; (f). Vertical angular intensity at $d = 50mm$.

4. Conclusion

In conclusion, we have proposed an efficient approach to convert THz Gaussian beam to top-hat beam and validated it by the backing experimental results. Our design process, based on iterative phase retrieve algorithm, is very simple and efficient. Moreover, our beam shaping system has only two phase plates, implying that it doesn't need a well aligned collimated input Gaussian beam. Finally, it is worthy noted that our approach is appropriate for generating THz beam with any desired intensity distribution due to the universality of phase retrieve algorithm and 3D-printing technology.

Funding

National Natural Science Foundation of China (NSFC) (61475054, 11574105).

References

1. M. Shalaby, C. Vicario, and C. P. Hauri, "Single-silicon CCD-CMOS platform for multi-spectral detection from terahertz to x-rays," Opt. Lett. **42**(22), 4596–4599 (2017).
2. C. Chevalier, L. Mercier, F. Duchesne, L. Gagnon, B. Tremblay, M. Terroux, F. Genereux, J.-E. Paultre, F. Provencal, Y. Desroches, L. Marchese, H. Jerominek, C. Alain, and A. Bergeron, "Introducing a 384x288 pixel terahertz camera core," Terahertz, RF, Millimeter, Submillimeter-Wave Technol. Appl VI. **8624**, 86240F (2013).
3. J. Oden, J. Meilhan, J. Lalanne-Dera, J. F. Roux, F. Garet, J. L. Coutaz, and F. Simoens, "Imaging of broadband terahertz beams using an array of antenna-coupled microbolometers operating at room temperature," Opt. Express **21**(4), 4817–4825 (2013).
4. K. B. Cooper, R. J. Dengler, N. Llombart, B. Thomas, G. Chattopadhyay, and P. H. Siegel, "THz imaging radar for standoff personnel screening," IEEE Trans. Terahertz Sci. Technol. **1**(1), 169–182 (2011).
5. E. Cristofani, F. Friederich, S. Wohnsiedler, C. Matheis, J. Jonuscheit, M. Vandewal, and R. Beigang, "Nondestructive testing potential evaluation of a terahertz frequency-modulated continuous-wave imager for composite materials inspection," Opt. Eng. **53**(3), 031211 (2014).

OSA CONTINUUM

6. H. Zhang, S. Sfarra, K. Saluja, J. Peeters, J. Fleuret, Y. Duan, H. Fernandes, N. Avdelidis, C. Ibarra-Castanedo, and X. Maldague, "Non-destructive Investigation of Paintings on Canvas by Continuous Wave Terahertz Imaging and Flash Thermography," J. Nondestruct. Eval. **36**(2), 34 (2017).
7. J. L. Kreuzer, "Coherent light optical system yielding an output beam of desired intensity distribution at a desired equiphase surface," US Patent 3,476,463 (1969).
8. H. Ma, Z. Liu, P. Zhou, X. Wang, Y. Ma, and X. Xu, "Generation of flat-top beam with phase-only liquid crystal spatial light modulators," J. Opt. A, Pure Appl. Opt. **12**, 045704 (2010).
9. R. Kleindienst, L. Moeller, and S. Sinzinger, "Highly efficient refractive Gaussian-to-tophat beam shaper for compact terahertz imager," Appl. Opt. **49**(10), 1757–1763 (2010).
10. F. S. Roux, "Intensity distribution transformation for rotationally symmetric beam shaping," Opt. Eng. **30**(5), 529 (1991).
11. J. W. Goodman, Introduction to Fourier Optics (Roberts and Company Publishers, 2005).
12. C. Liu, L. Niu, K. Wang, and J. Liu, "3D-printed diffractive elements induced accelerating terahertz Airy beam," Opt. Express **24**(25), 29342–29348 (2016).
13. C. C. Aleksoff, K. K. Ellis, and B. D. Neagle, "Holographic conversion of a Gaussian beam to a near-field uniform beam," Opt. Eng. **30**(5), 537–543 (1991).
14. X. Wei, C. Liu, L. Niu, Z. Zhang, K. Wang, Z. Yang, and J. Liu, "Generation of arbitrary order Bessel beams via 3D printed axicons at the terahertz frequency range," Appl. Opt. **54**(36), 10641–10649 (2015).
15. D. L. Shealy and J. A. Hoffnagle, "Laser beam shaping profiles and propagation," Appl. Opt. **45**(21), 5118–5131 (2006).
16. D. L. Shealy, J. A. Hoffnagle, and K.-H. Brenner, "Analytic beam shaping for flattened output irradiance profile," in Laser Beam Shaping VII, Vol. **6290**, p. 629006. (2006)
17. R. W. Gerchberg and W. O. Saxton, "A practical algorithm for the determination of phase from image and diffraction plane pictures," Optik (Stuttg.) **35**, 237–246 (1972).
18. J. R. Fienup, "Phase retrieval algorithms: a comparison," Appl. Opt. **21**(15), 2758–2769 (1982).
19. G. Z. Yang, B. Z. Dong, B. Y. Gu, J. Y. Zhuang, and O. K. Ersoy, "Gerchberg-Saxton and Yang-Gu algorithms," Appl. Opt. **33**(2), 209–218 (1994).
20. R. Tommasini, F. Löwenthal, J. E. Balmer, and H. P. Weber, "Iterative method for phase-amplitude retrieval and its application to the problem of beam-shaping and apodization," Opt. Commun. **153**(4-6), 339–346 (1998).
21. J. R. Fienup, "Iterative method applied to image reconstruction and to computer-generated holograms," Opt. Eng. **19**(3), 193297 (1980).
22. J. A. Marozas, "Fourier transform-based continuous phase-plate design technique: a high-pass phase-plate design as an application for OMEGA and the National Ignition Facility," J. Opt. Soc. Am. A **24**(1), 74–83 (2007).
23. J. A. Hoffnagle and C. M. Jefferson, "Design and performance of a refractive optical system that converts a Gaussian to a flattop beam," Appl. Opt. **39**(30), 5488–5499 (2000).